RSC Advances

PAPER

View Article Online
View Journal | View Issue

Cite this: *RSC Adv.*, 2024, **14**, 3480

Acid–base equilibrium in non-aqueous medium: colorimetric visualization, estimation of acidity constants and construction of molecular logic gates†

Manas Mahato, Arpita Maiti, Sabbir Ahamed, Madan Rajbanshi, Shubham Lama and Sudhir Kumar Das *

A reversible acid–base probe, (N^1E, N^4E)-N^1, N^4-bis((*Z*)-3-(4-(dimethylamino)phenyl)allylidene)benzene-1,4-diamine (**MM1**), is introduced for the colorimetric visualization of acid–base equilibria in non-aqueous media. **MM1** displays reversible acidochromic behavior, showing exciting colorimetric change varying from weak to strong acid. Also, we have fabricated a colorimetric paper strip-based test kit to visualize acid–base equilibria. A dipstick experiment has been demonstrated to visualize the acid–base equilibria in the gaseous state. This acid–base probe has also been employed to estimate the pK_a values of several acidic compounds in a non-aqueous medium using overlapping indicator methods. Based on reversible acidochromic UV-visible absorption spectral and colorimetric behavior, we have constructed a reconfigurable dual input and dual output combinational logic circuit and set-reset memorized device employing acid and base as chemically encoded inputs and corresponding optical outputs. The current report evokes a new protocol for developing various reversible acidochromic probes and its implication for constructing opto-chemical molecular logic gates and estimating the acid dissociation constants of various acidic compounds in non-aqueous media.

Received 13th July 2023
Accepted 9th January 2024

DOI: 10.1039/d3ra04696f

rsc.li/rsc-advances

1. Introduction

Acidity is one of the most significant phenomena crucial to nature; even living organisms have a sense of it.[1,2] The proton is undoubtedly one of the most fundamental particles for a chemist. The acid–base reaction, frequently studied in aqueous to polar media, *i.e.*, media with ionizable protons that allow for a simple evaluation, is one of the ubiquitous reactions related to acidity and basicity (*e.g.*, potentiometry, conductometry). Most chemical reactions, such as acid-catalyzed reactions in the laboratory and the industry, occur in non-aqueous media because the replaced arenes, alkanes, ethers, or haloalkanes[3] have appropriate dielectric constant (ε_r) values between 2 and 14. For this reason, nonpolar, non-aqueous mediums have been employed for performing acid-catalyzed reactions in the laboratory.[4] Hence, it is paramount to comprehend the acid–base chemistry in nonpolar, non-aqueous media rather than aqueous media.

At the same time, many areas of science and engineering research depend on the ability to visualize the acid–base equilibrium process. It regulates a variety of chemical and biological processes that take place in aqueous, non-aqueous, and gaseous media. Additionally, it is fundamentally necessary to design and develop various functional materials, including catalysts,[5,6] sensors,[7] proton conductive membranes,[8,9] *etc.* To detect tiny quantities of acid–base in aqueous and non-aqueous media, a variety of acid–base sensors, including indicator reagents or strips, pH electrodes (hydrogen electrode, quinhydrone electrode, antimony electrode, glass electrode), and optical sensors, have recently arrived on the market. Among the different acid–base detectors, optical sensors[10–25] have drawn much interest because of their potential for efficiency, resistance to electrical curiosity, and capacity for unreachable sensing. However, it has been reported that several organic dyes can function as colorimetric sensors in non-aqueous solutions.[12–17,22–25] Although these sensors make it possible to estimate the concentrations of colorless acids or bases, they have not yet been used to calculate the acid dissociation constant, which is crucial for comprehending the acid–base chemistry in those mediums.[26–32] To comprehend the non-aqueous acid–base chemistry, it is urgent to determine the acid dissociation constant with newly developed chromophoric systems that include electron donor–acceptor subunit. The design and development of such an acid–base sensor to observe acid–base equilibrium occurring in a non-aqueous medium and

Department of Chemistry, University of North Bengal, Darjeeling, West Bengal 734013, India. E-mail: sudhirkumardas@nbu.ac.in

† Electronic supplementary information (ESI) available. See DOI: https://doi.org/10.1039/d3ra04696f

potentially determine the trace quantities of acids and bases in non-aqueous nonpolar media are fundamentally important.[17]

The acid dissociation constant is the most critical and valuable research parameter.[27–35] Numerous studies have been conducted to determine the acid dissociation constant in protic solvents, but few have been shown in less polar aprotic solvents.[27,28,33–36] When performing acid-catalyzed organic reactions, it is crucial to understand an acid's dissociation constants in the non-aqueous, aprotic, nonpolar medium. The electrostatic attraction between the proton and the conjugate base of an acid can be reduced by the solvents with high dielectric constant, allowing them to be separated in the solvent.[33,37] However, this dissociation of acid is unfavorable in less polar solvents. So far, researchers have shown great interest in determining the degree of acid dissociation in less polar solvents. Most of the time, measurements have been performed conductometrically or potentiometrically with glass electrodes, which involves numerous presumptions during the measurement process.[33,36,37] The most effective way for determining the prototropic dissociation constant of an acid or base in the aprotic less-polar solvents employing some indicators applying overlapping indicator method in order to avoid those related issues.[33,38,39]

Because of its many characteristics, acetonitrile (ACN) is a good choice for pK_a value estimation of strong acids. It has an inferior ability to solvate anions and poor basicity.[40] The low basicity of ACN is an advantage over the other commonly used solvents for acid–base investigations, water and DMSO, which are significantly more basic (stronger acceptors of hydrogen bonds) and thus act as leveling solvents for strong acids. Ion pairs are more likely to break apart into free ions in ACN due to their high relative permittivity ($D = 36.0$).[40] The autoprotolysis constant (K_{auto}) of ACN has been calculated to be as extremely low as 33 (ref. 41) (although values as high as 44 have been proposed).[42,43] Its combination of all these characteristics makes it an effective distinguishing solvent for strong acids.

With the aforementioned information in mind, we have introduced a superior chromogenic sensor **MM1** using the handy condensation of 1,4-phenylenediamine and 4-dimethylaminocinnamaldehyde, which is extremely sensitive and selective towards acid, and results in visible color changes from yellow to violet in an acetonitrile medium. Interestingly, the visible colorimetric change is entirely reversible due to the treatment with a base under the same experimental conditions, augmenting the visualization of acid–base equilibria in the non-aqueous medium. A portable test kit employing **MM1** coated with filter paper has been fabricated to visualize the acid–base equilibria in the solution and gaseous phase, respectively. The excellent colorimetric reversibility makes it an ideal candidate for the construction of various logic gate operators, which could be helpful for the fabrication of various opto-chemical devices. The developed chromogenic sensor has also been utilized to estimate the K_a values of numerous weak to strong acids in a non-aqueous medium. This report presents a practical approach for developing a colorimetric chemosensor for the selective detection and quantification of acid–base in non-aqueous media. Thus, the present contribution represents a complete account of a newly developed reversible acidochromic behavior of an acid–base probe and its implication for determining the acidity of several acidic compounds and constructing various opto-chemical molecular logic gates.

2. Experimental sections

2.1 Reagents and solvents

All the reagents, including 1,4-phenylenediamine and 4-dimethylamino cinnamaldehyde, are purchased from TCI and Sigma Aldrich, India, respectively. All the HPLC-grade solvents and acids are bought from Merck, India. The solvents are dried before each spectrophotometric investigation. All the glassware is meticulously cleaned with concentrated sulfochromic acid, then washed several times with distilled water, and finally washed with acetone.

2.2 Preparation of stock solutions

One mM concentration of **MM1** is prepared as a stock solution in an ACN medium. As well as all the acids and bases are prepared at one mM of concentration by dissolving appropriate amounts in ACN.

2.3 Instrumentations

UV-visible absorption spectra are recorded with the help of HITACHI U-2910. ^{1}H-NMR and ^{13}C-NMR spectra are carried out with the help of Bruker 400 MHz instrument at ambient atmospheres using tetramethylsilane (TMS) as a standard reference with chemical shifts (δ) in ppm unit. An Agilent 6545XT AdvanceBio LC/Q-TOF spectrometer has been used to carry out the high-resolution mass spectra (HRMS).

2.4 Synthesis of MM1 and characterization

Our target acid–base probe, (N^1E, N^4E)-N^1, N^4-bis((*Z*)-3-(4-(dimethylamino)phenyl)allylidene)benzene-1,4-diamine (**MM1**) has been synthesized by the simply condensation reaction of 1,4-phenylenediamine and 4-dimethylamino cinnamaldehyde in an acidic medium (Scheme 1). 1,4-Phenylenediamine (50 mg, 0.4623 mmol) is taken in a round bottom flask and dissolved with 3 ml of methanol, then 4-dimethylaminocinnamaldehyde (162 mg, 0.9247 mmol) is added and stirred the reaction mixture along with the added catalytic amount of acetic acid. The reaction mixture is refluxed for around 6 h at 60 °C. The reddish-brown color product is collected and washed in hot methanol several times, and the product is dried in a hot air oven at 60 °C. Yield = 89%.

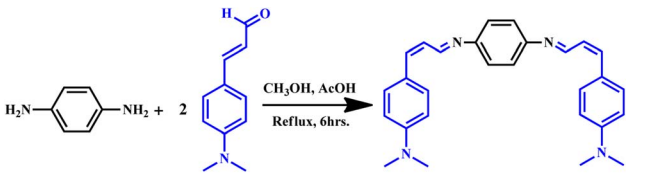

Scheme 1 Synthetic procedure of MM1.

2.4.1 Characterization. ^{1}H NMR (400 MHz, δ, ppm; $CDCl_3$); (Fig. S1†): 8.29 (d, –CH═N, 1H), 7.45 (d, 1H), 7.21 (s, 2H), 7.10 (d, 2H), 6.98 (dd, 2H), 6.71 (d, 2H) 3.02 (s, 6H). ^{13}C NMR (100 MHz, δ, ppm; $CDCl_3$); (Fig. S2†): 161.46, 151.31, 149.74, 144.64, 129.06, 124.12, 121.80, 112.04, 40.19 and from the high-resolution mass spectra (Fig. S3†) m/z is found to be 423.2547(**MM1** + H^+, calculated 423.2555) confirming the formation of our **MM1**.

3. Results and discussions

3.1 UV-visible spectrophotometric and colorimetric analysis

We have conducted a UV-visible spectrophotometric titration experiment with the gradual additions of acid into the solution of **MM1** in ACN to check the detecting ability of our chromogenic probe towards acid. **MM1** exhibits broadband from 300 nm to 500 nm, having a maximum at 416 nm in the UV-visible absorption spectra, which is intramolecular charge transfer (ICT) in nature. An extended charge delocalization from the *N*,*N*-dimethylamino group of cinnamylamine to the benzene ring of 1,4-phenylene diamine occurs, which is responsible for the UV-visible spectral behavior. We have chosen acetic acid and trifluoro acetic acid as representative examples of weak and strong acids for performing the UV-visible spectrophotometric titration experiment. Upon gradual addition of acetic acid (0–0.2 M) into the **MM1** solution, the absorbance intensity of the peak of our free sensor, located at 416 nm, is gradually decreased. Simultaneously, a new peak is generated at 544 nm (Fig. 1a) which is due to the extended delocalization into our probe **MM1** displaying a clear isosbestic point located at 474 nm, indicating the acidified and nonacidified **MM1** probe is in equilibrium process in the solution. The equilibrium process between protonated and deprotonated **MM1** is also manifested in the change in absorbance values at 416 nm and 544 nm, respectively (Fig. 1b). A noticeable apparent colorimetric change from yellow to pink (Fig. 1a inset) is observed due to the acidification of our probe, **MM1**. Interestingly, upon gradual addition of trifluoro acetic acid (0–33.6 μM) into the **MM1** solution, it is observed that the absorbance intensity gradually decreases at 416 nm with a simultaneous generation of new peak located at 566 nm up to the introduction of 33.6 μM TFA which is due to the highly extended charge transfer into our probe **MM1** (Fig. 1c). Interestingly due to the further introduction of TFA, the peak position located at 566 nm is slightly red-shifted, generating a new hump situated at 630 nm, which is also manifested from the chronological colorimetric change of the **MM1** solution to the introduction of TFA. A noticeable isosbestic point is observed at 474 nm, indicating that the protonation process is at equilibrium in the solution, which is also evident from the change in absorbance values at 416 nm and 566 nm, respectively. The initial color of the **MM1** solution changes from yellow to pink, then purple, and finally blue (Fig. 1c inset). The difference in colorimetric change is probably due to the number of protonations of the **MM1** in the solution.

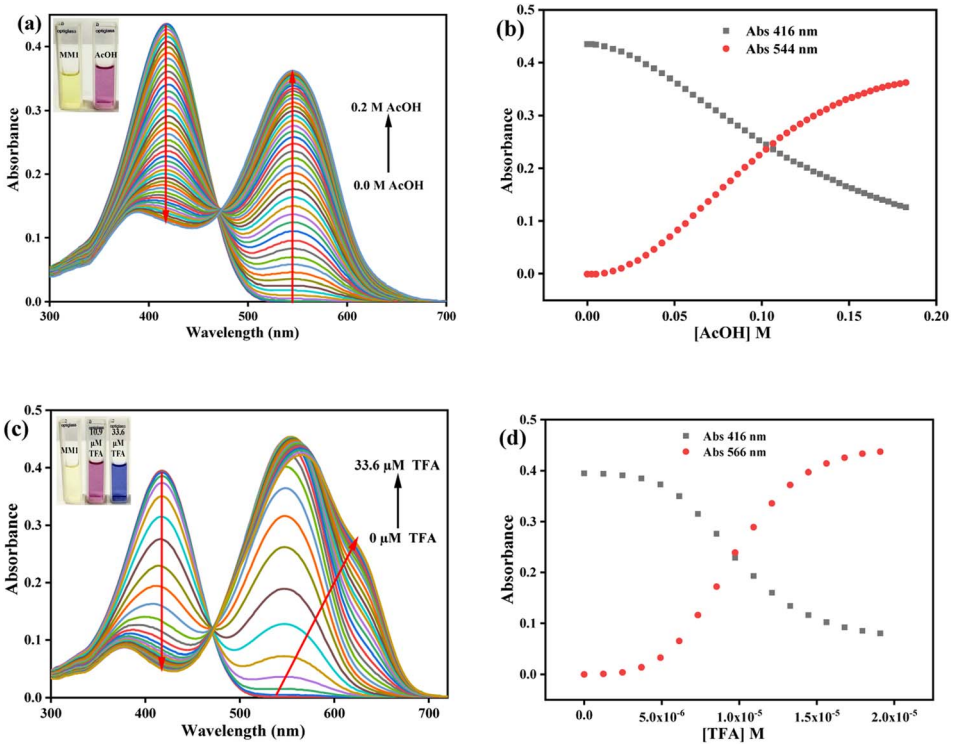

Fig. 1 UV-visible absorption titration spectra of MM1 (7.44 μM) due to the gradual addition of (a) weak acid (acetic acid, in set: demonstrate the colorimetric change of MM1 solution due to the introduction of acetic acid) and (c) strong acid (trifluoro acetic acid, photo inset shows the colorimetric change of MM1 solution due to the introduction of TFA) in pure acetonitrile medium. Ratiometric changes of absorbance intensity with increasing concentration of (b) weak and (d) strong acids.

In the case of the weak acid, due to the monoprotonation, one symmetrical part of the **MM1** is transferred from imine to quinonoid, which is probably due to the colorimetric change from yellow to pink coloration of the **MM1** solution. On the other hand, protonation occurs sequentially in the presence of TFA. Due to the addition of 10.9 μM TFA, monoprotonation of **MM1** occurs, which is responsible for the colorimetric change from yellow to pink. Due to the further addition of TFA, double protonation of **MM1** occurs, and the color of the **MM1** solution gradually changes from pink to purple and finally to blue. From these observations, it could be inferred that the acid dissociation constant plays a vital role in the colorimetric visualization of acid–base equilibria in the non-aqueous media. If the acid is weak in nature, one could observe pink coloration, and if it is robust in nature, one could notice a gradual color change from yellow to pink, then purple, and finally blue. To understand the protonation behavior of **MM1**, we performed ^{1}H NMR titration with the addition of acetic acid. The protonation of the –CH═N unit leads to a doublet peak located at 9.6 ppm following the introduction of AcOH into the **MM1** solution in $CDCl_3$, confirming the protonation site is an imine proton. Furthermore, the protons situated between the cinnamylamine unit and the nitrogen atoms of the terminals experience a shift toward the lower field (Fig. 2).

3.2 Reversibility investigation

Reversibility is the main characteristic of an ideal acid–base indicator. Our probe **MM1** shows reversible acidochromism due to the consecutive introduction of acid and base. To establish the reversible acidochromism behavior of our probe, **MM1**, we have performed the reversible UV-visible spectrophotometric titration experiment upon introducing triethyl amine (TEA) into the **MM1** acidic solution. Interestingly, upon gradual addition of TEA into the weak acid acidified **MM1** solution, the absorbance intensity of the peak located at 544 nm decreased gradually with the simultaneous enhancement of absorbance values at 416 nm due to the transformation quinoid to imine from our probe **MM1** (Fig. S4†). A pronounced colorimetric change from pink to yellow coloration is noticed. Interestingly, the same reversible phenomena are observed in robust acid-acidified **MM1** solution (Fig. 3a). First, the hump peak located at 630 nm is gradually vanishing with the reduction of absorbance values of the peak located at 656 nm with the simultaneous enhancement of absorbance values at the peak located at 416 nm. A reverse sequential colorimetric change from blue to purple, then pink, and finally into the original color of **MM1** (Fig. 3b). From these findings, we can conclude that we can reuse our probe, **MM1**, multiple times for sequential identification of acid–base. Interestingly, our synthesized sensor **MM1** exhibits five reversible cycles in ACN medium upon cascade addition with TFA and TEA, as shown in Fig. 3c. Therefore, the probe **MM1** could be used as a proficient ideal acid–base indicator in the non-aqueous medium.

3.3 Application as solid-state acid–base sensor

Due to the flexibility of chemosensors, test kits based on low-cost materials have recently drawn the most attractive to the scientific community in the field of sensing research in place of applying sophisticated, costly apparatus and time-consuming experimental methodologies; in other words, the main limitations of the practical usability of chemosensors are their expensive instrumentation and lengthy experimental procedures. Keeping the above fact in mind, we have fabricated a paper strip-based test kit for the sequential detection of acid and base without any expensive instrument and without any waste of time. We took the Whatman-41 paper strip and dipped it in the **MM1** solution (1 mM), then dried it in a hot air oven at 60 °C. After drying, the yellow color paper strip is dipped into TFA solution (0.5×10^{-3} M). We have found that the instant color changes from yellow to blue due to the protonation of **MM1**, which is reversed in the presence of a base, TEA (Fig. 4a). We have also performed the same experiment in the various concentrations of TFA and observed the color

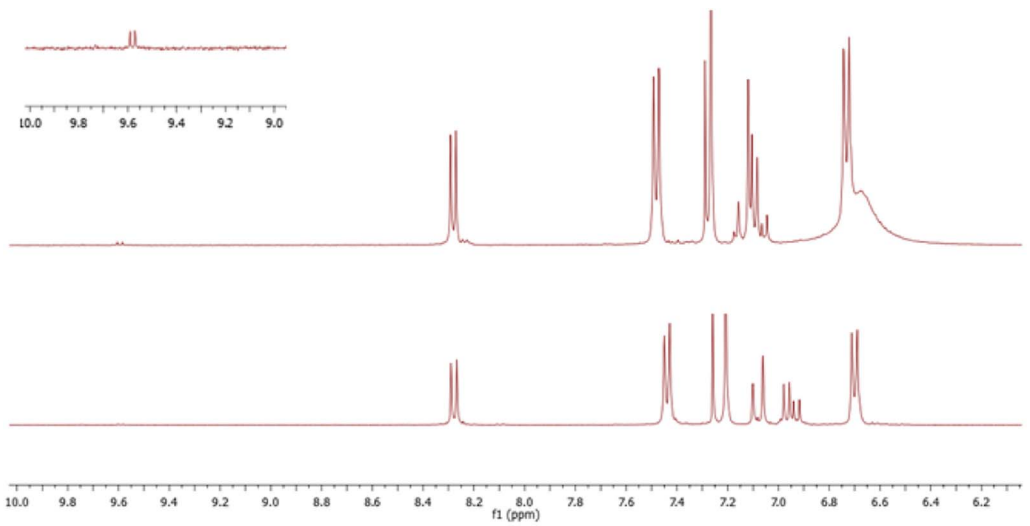

Fig. 2 ^{1}H NMR titration spectra of MM1 with the addition of acetic acid.

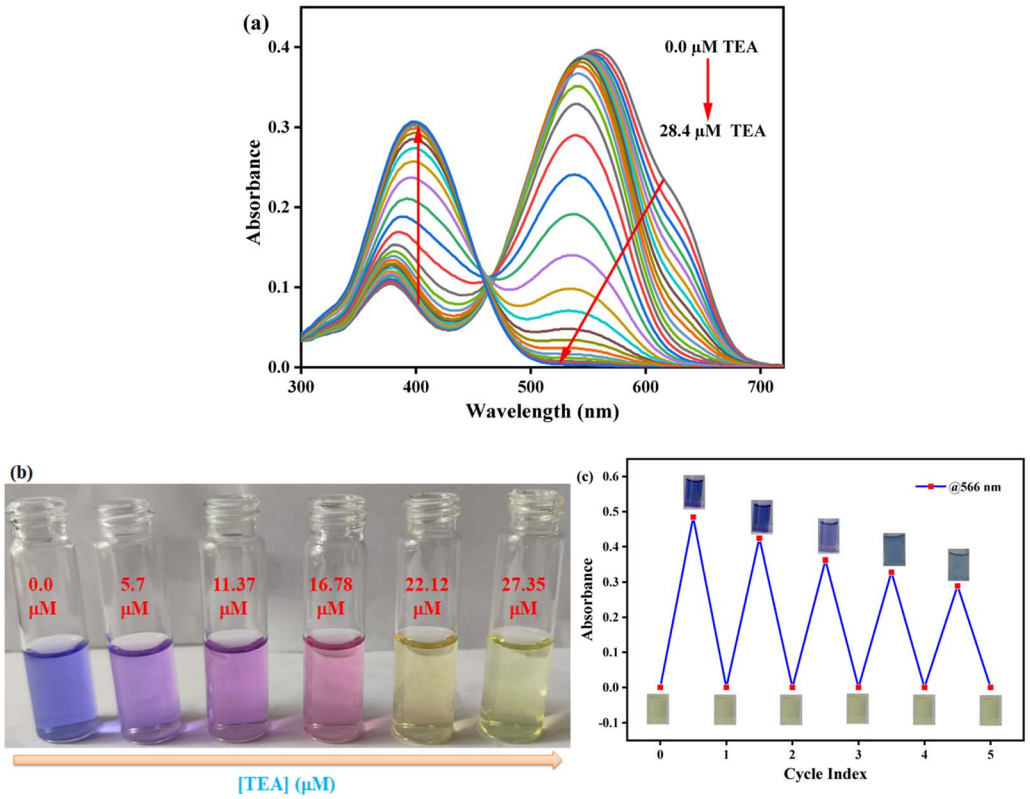

Fig. 3 (a) The UV-visible absorption reversible titration spectra of strong acid acidified **MM1** upon steady addition of TEA (0–28.4 μM) in pure acetonitrile solvent. (b) Color change observation after the addition of TEA. (c) Reversible cycle after sequential addition of TFA and TEA in the **MM1** solution.

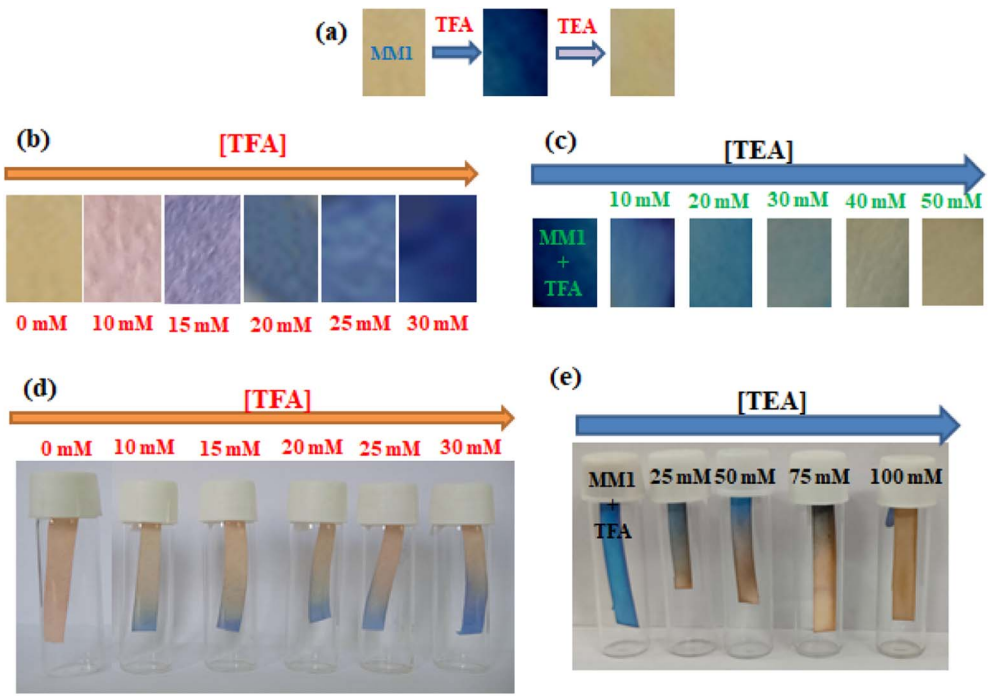

Fig. 4 (a) Pictorial representation of the colorimetric change of **MM1**-stained paper strips upon introducing TFA and TEA sequentially. Colorimetric change of **MM1**-stained paper strips upon exposure to various concentrations of (b) TFA and (c) TEA. Colorimetric change of **MM1**-stained paper strips upon exposure to numerous concentrations of (d) TFA vapor and (e) TEA vapor.

changes from yellow to pink, purple, and finally blue (Fig. 4b), demonstrating its usefulness in quantifying the concentration of strong acid, although its entirely depend on the supplying capability of protons. Interestingly, when we dipped the strip into the TEA solution (1×10^{-3} M), the color was fully reversed to the original color (blue to yellow) of **MM1** due to the deprotonation of **MM1** (Fig. 4c). We have also executed a dipstick method for its practical utility for detecting acid and base in the gaseous phase. We have exposed the paper strips to various concentrations of TFA vapor. Interestingly, it changed its color from yellow to blue (Fig. 4d); further exposure to the TEA vapor came to the original yellow color (Fig. 4e). From this observation, we can conclude that our fabricated paper strip-based test kit can be used for practical purposes with low-cost, fast-responsive, and on-spot detection of acid and base sequentially in solid and gaseous states, respectively.

3.4 Estimation of pK_a values of acids in the non-aqueous medium

The acidochromic behavior of **MM1** has been utilized to estimate the equilibrium acidities of several acids by using spectrophotometric titration in an ACN medium. The determination of the pK_a values of various acids in a non-aqueous medium has been documented in numerous reports.[20–22] The most common techniques used are conductometric or potentiometric, with glass electrodes serving as the reference electrodes.[34–36] Based on some presumptions, a theoretical calculation in the non-aqueous medium is made to determine the relationship between the acidity and the formal potential values of the glass electrode. Thus, the method of determination might not be the most accurate one.[26] There is currently a lack of understanding regarding acidity and the quantifiable calculation of the acid–base equilibrium constant in a non-aqueous medium. The best method for calculating an acid's equilibrium constant in non-aqueous solvents is to use an acidochromic probe.[44,45] It is simple to determine the acidity of a medium spectrophotometrically using a probe with an understanding of its equilibrium constant (pK_{Ind}) values. Analyte concentrations in these spectrophotometric studies are kept as low as possible to prevent any undesirable clashing processes. Using the overlapping indicator method developed by Bordwell *et al.* for a non-aqueous aprotic medium, the pK_a of an undetermined acid–base composite has been determined in the non-aqueous medium (the detailed procedures are provided in the ESI†).[27,39] Here, by carefully observing the spectroscopic shift of the **MM1** throughout the spectrophotometric titration procedure at ambient conditions (Fig. S6–S10 and Table S1†), the pK_a values of several commonly used acids in comparison to that of the **MM1** probe (pK_{Ind}) (Fig. S5†) have been determined in pure ACN medium. The calculated values of the acidity constants have been determined to agree with the values from the literature (Table 1).

3.5 Molecular logic gate construction

Our synthesized **MM1** displays a reversible colorimetric acidochromism, enabling the visualization of acid–base equilibria in the non-aqueous media. We have found that **MM1** responds strongly to TFA in an acetonitrile solution, showing a distinct colorimetric behavior that reverses in the presence of TEA. Using this acid–base as the inputs' chemical encoding and the corresponding optical outputs, a combinational logic circuit has been constructed based on the comeback profiles of the sensor **MM1** as measured by absorbance values towards TFA and TEA at specific wavelengths in pure ACN medium. To build the logic circuit with two optical outputs concerning absorbance value at 416 nm (output 1) and absorbance value at 566 nm (output 2) for **MM1** where TFA (input 1) and TEA (input 2) have been used as chemical encoded inputs, it is assumed that the threshold absorbance values for outputs 1 and 2 are 0.165 and 0.119, respectively. Boolean 1 represents an absorbance value above the threshold, and boolean 0 represents one below the threshold. Now, the output signal at 416 nm signifies an IMPLY (IMP) arrangement where the optical density value is deficient (*i.e.*, 0) only with TFA. In contrast, the signal at 566 nm is similar to that of the INHIBIT (INH) logic gate arrangement where the optical density value is high (*i.e.*, 1). A combined logic circuit with two chemically encoded inputs and corresponding optical outputs is constructed using these two logic gates. UV-visible spectral changes and absorbance values change of probe-**MM1** at 416 and 566 nm, respectively, in ACN, pictorial representation combinational logic circuit, corresponding "truth table" for the formation of a combinational logic circuit, and demonstration of colorimetric visualization of **MM1** solution for the formation of the opto-chemical combinational logic circuit are shown in Fig. 5.

Table 1 Estimation of pK_a values of several acids at room temperature in acetonitrile

Acids	pK_a values[a] in acetonitrile
TFA	12.55 (12.60)[46]
Formic acid	17.70 (20.30)[47]
Salicylic acid	15.00 (16.70)[35]
Oxalic acid	15.37 (15.97)[48]

[a] In the bracket contains literature values.

3.6 Design of opto-chemical molecular memory device

Data processing and storage at the molecular level is crucial in the modern computer era and requires the operation of successive molecular logic circuits. One of the outputs is treated as an input and memorized as a memory element in the logic circuit's feedback loop, which controls operation. Herein, we have constructed a memory device with a "write–read–erase–read" type of behavior using the protonation of the sensor **MM1**, followed by its reversibility by deprotonation through UV-visible spectrophotometric and colorimetric signaling. In this designed opto-chemical memory device system, we have chosen input 1 as TFA, whereas input 2 is TEA. The acidified **MM1** system forms an initial absorption peak at 566 nm at the addition of excess TFA because the fully protonated probe **MM1** is produced. It is a "set process" in which the entire system

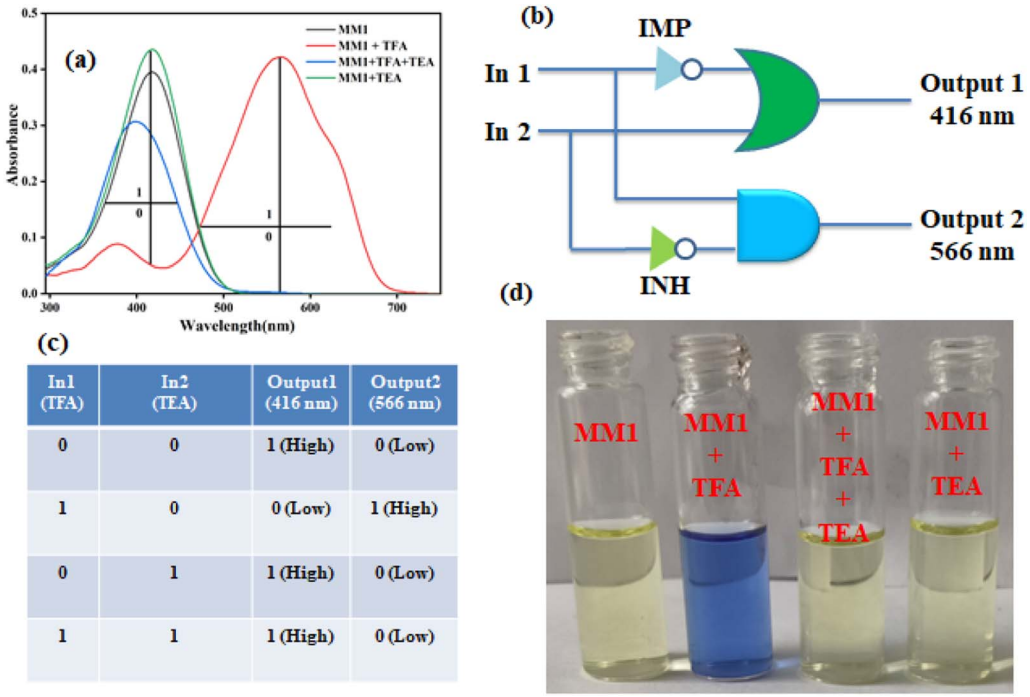

In1 (TFA)	In2 (TEA)	Output1 (416 nm)	Output2 (566 nm)
0	0	1 (High)	0 (Low)
1	0	0 (Low)	1 (High)
0	1	1 (High)	0 (Low)
1	1	1 (High)	0 (Low)

Fig. 5 (a) UV-visible spectral changes and absorbance values change of probe-**MM1** at 416 and 566 nm, respectively, in ACN; (b) pictorial representation combinational logic circuit; (c) the matching truth table for the formation combinational logic circuit; (d) demonstration of the colorimetric visualization of **MM1** solution for forming the opto-chemical combinational logic circuit.

writes and reads the resulting signal as binary 1. With the addition of TEA, the peak at 566 nm is now diminished due to the formation of the completely deprotonated probe **MM1**. This is a "reset process" in which the system is cleared, and the resulting signal is read as binary 0. The UV-visible spectral changes of probe-**MM1** at 566 nm in ACN and corresponding

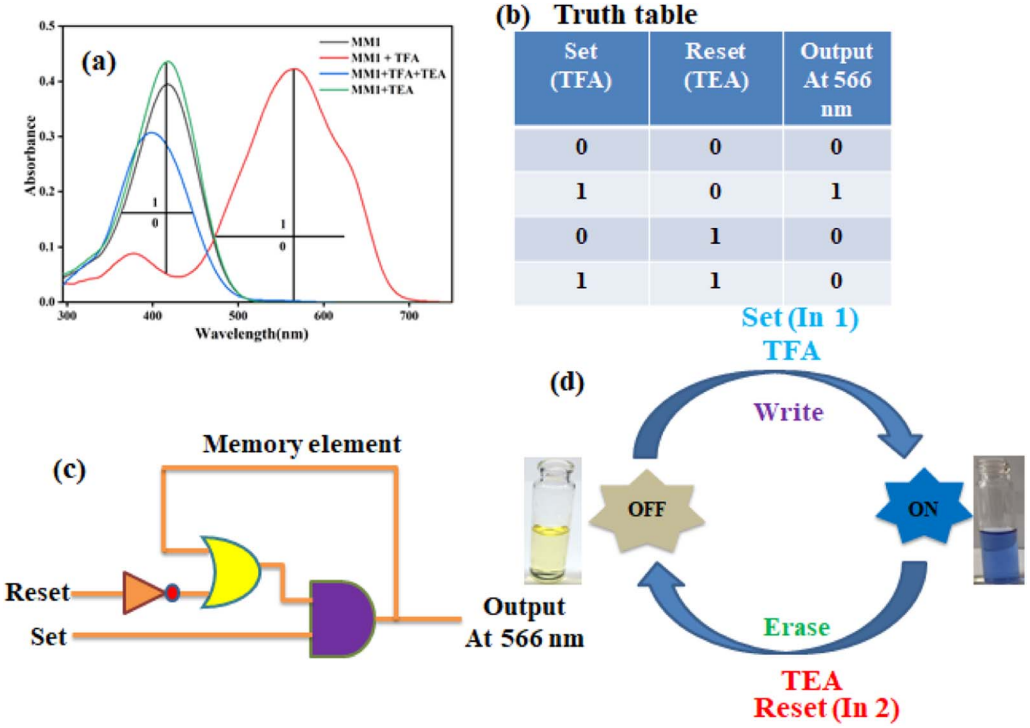

Set (TFA)	Reset (TEA)	Output At 566 nm
0	0	0
1	0	1
0	1	0
1	1	0

Fig. 6 (a) UV-visible spectral changes and absorbance values change of probe-**MM1** at 566 nm in ACN; (b) corresponding "truth table" for the formation of "memorised device"; (c) pictorial demonstration of the logic circuit of the "memory device"; and (d) demonstration of reversible logic operations with "writing–reading–erasing–reading" behavior.

"truth table" for the formation of the "memorised device," pictorial representation of the logic circuit of the "memory device," and demonstration of reversible logic operations with "writing–reading–erasing–reading" behavior is displayed in Fig. 6.

4. Conclusion

In conclusion, we have successfully introduced an acid–base indicator, **MM1**, for the non-aqueous medium. **MM1** displays reversible acidochromic behavior, showing exciting colorimetric change varying from weak to strong acid. Further, the developed acid–base indicator estimates the pK_a values of numerous acidic compounds in a non-aqueous medium. Based on the reversible UV-visible spectrophotometric and colorimetric behavior, we have constructed a molecular logic circuit and set-reset memory device using the TFA and TEA as chemically encoded inputs and corresponding optical output. We have fabricated a paper strip-based test kit to visualize acid–base equilibria for practical utility. A dipstick method has also been employed to visualize acid–base equilibria in the gaseous medium. Overall, the present article provides a distinct perspective on developing reversible acidochromic behavior of newly synthesized compounds and its application for constructing various opto-chemical molecular logic circuits and determining acid dissociation constants in the non-aqueous media.

Conflicts of interest

There are no conflicts of interest to declare.

Acknowledgements

SKD is grateful to SERB, New Delhi, Govt. of India (EEQ/2019/000054) for their financial support, without which this research would not have been possible. We also thank the University Grants Commission (UGC) (Start-up Research grant), New Delhi, for the generous research grant. MM, SA thank Govt. of West Bengal, India, for the Swami Vivekananda Merit-cum-Means Scholarship awarded to them.

References

1 S. Arrhenius, *Z. Phys. Chem.*, 1887, **1U**, 631–648.
2 J. N. Brönsted, *Recl. Trav. Chim. Pays-Bas*, 1923, **42**, 718–728.
3 H. Clavier and H. Pellissier, *Adv. Synth. Catal.*, 2012, **354**, 3347–3403.
4 E. Paenurk, K. Kaupmees, D. Himmel, A. Kütt, I. Kaljurand, I. A. Koppel, I. Krossing and I. Leito, *Chem. Sci.*, 2017, **8**, 6964–6973.
5 Z. Zhu, M. Odagi, C. Zhao, K. A. Abboud, H. U. Kirm, J. Saame, M. Lõkov, I. Leito and D. Seidel, *Angew. Chem., Int. Ed.*, 2020, **59**, 2028–2032.
6 Q. Deng, X. Li, R. Gao, J. Wang, Z. Zeng, J. J. Zou, S. Deng and S. C. E. Tsang, *J. Am. Chem. Soc.*, 2021, **143**, 21294–21301.
7 J. Han and K. Burgess, *Chem. Rev.*, 2010, **110**, 2709–2728.
8 J. F. Huang, H. Luo, C. Liang, I. W. Sun, G. A. Baker and S. Dai, *J. Am. Chem. Soc.*, 2005, **127**, 12784–12785.
9 C. Ke, J. Li, X. Li, Z. Shao and B. Yi, *RSC Adv.*, 2012, **2**, 8953–8956.
10 H. H. Cho, S. H. Kim, J. H. Heo, Y. E. Moon, Y. H. Choi, D. C. Lim, K. H. Han and J. H. Lee, *Analyst*, 2016, **141**, 3890–3897.
11 C. Smyth, K. T. Lau, R. L. Shepherd, D. Diamond, Y. Wu, G. M. Spinks and G. G. Wallace, *Sens. Actuators, B*, 2008, **129**, 518–524.
12 S. Banthia and A. Samanta, *J. Phys. Chem. B*, 2006, **110**, 6437–6440.
13 A. Maity, P. Mazumdar, S. Samanta, D. Das, M. Shyamal, G. P. Sahoo and A. Misra, *J. Mol. Liq.*, 2016, **221**, 358–367.
14 G. Chakraborty, J. N. Malegaonkar, S. V. Bhosale, P. K. Singh and H. Pal, *J. Phys. Chem. B*, 2021, **125**, 11122–11133.
15 J. Kaur, D. Bandyopadhyay and P. K. Singh, *J. Mol. Liq.*, 2022, **347**, 118258.
16 J. Kaur and P. K. Singh, *Sens. Actuators, B*, 2021, **346**, 130517.
17 A. Shundo, S. Ishihara, J. Labuta, Y. Onuma, H. Sakai, M. Abe, K. Ariga and J. P. Hill, *Chem. Commun.*, 2013, **49**, 6870–6872.
18 M. Elhabiri, O. Siri, A. Sornosa-Tent, A. M. Albrecht-Gary and P. Braunstein, *Chem.–Eur. J.*, 2004, **10**, 134–141.
19 Q. Zhang, S. Zhang, S. Liu, X. Ma, L. Lu and Y. Deng, *Analyst*, 2011, **136**, 1302–1304.
20 K. Y. Yung, A. J. S. Hewitt, N. P. Hunter, F. V. Bright and G. A. Baker, *Chem. Commun.*, 2011, **47**, 4775–4777.
21 W. I. S. Galpothdeniya, K. S. McCarter, S. L. De Rooy, B. P. Regmi, S. Das, F. Hasan, A. Tagge and I. M. Warner, *RSC Adv.*, 2014, **4**, 7225–7234.
22 R. Ali, S. M. Saleh and R. F. M. Elshaarawy, *RSC Adv.*, 2016, **6**, 86965–86975.
23 L. Gao, X. Lin, A. Zheng, E. Shuang, J. Wang and X. Chen, *Anal. Chim. Acta*, 2020, **1111**, 132–138.
24 M. Sarkar and A. Samanta, *J. Phys. Chem. B*, 2007, **111**, 7027–7033.
25 M. Sarkar, S. Banthia, A. Patil, M. B. Ansari and A. Samanta, *New J. Chem.*, 2006, **30**, 1557–1560.
26 I. M. Kolthoff, M. K. Chantooni and S. Bhowmik, *Anal. Chem.*, 1967, **39**, 1627–1633.
27 W. S. Matthews, J. E. Bares, J. E. Bartmess, F. J. Cornforth, G. E. Drucker, R. J. McCallum, G. J. McCollum, N. R. Vanier, F. G. Bordwell and Z. Margolin, *J. Am. Chem. Soc.*, 1975, **97**, 7006–7014.
28 E. Rossini, A. D. Bochevarov and E. W. Knapp, *ACS Omega*, 2018, **3**, 1653–1662.
29 S. N. Park, H. Kim, K. Kim, J. A. Lee and D. seok Lho, *Phys. Chem. Chem. Phys.*, 1999, **1**, 1893–1898.
30 T. Matsui, T. Baba, K. Kamiya and Y. Shigeta, *Phys. Chem. Chem. Phys.*, 2012, **14**, 4181–4187.
31 A. Kütt, I. Leito, I. Kaljurand, L. Sooväli, V. M. Vlasov, L. M. Yagupolskii and I. A. Koppel, *J. Org. Chem.*, 2006, **71**, 2829–2838.
32 I. M. Kolthoff, S. Bruckenstein and M. K. Chantooni, *J. Am. Chem. Soc.*, 1961, **83**, 3927–3935.

33 I. M. Kolthoff, M. K. Chantooni and S. Bhowmik, *Anal. Chem.*, 1967, **39**, 315–320.
34 G. Garrido, E. Koort, C. Ràfols, E. Bosch, T. Rodima, I. Leito and M. Rosés, *J. Org. Chem.*, 2006, **71**, 9062–9067.
35 H. S. Kim, T. D. Chung and H. Kim, *J. Electroanal. Chem.*, 2001, **498**, 209–215.
36 W. C. Barrette, H. W. Johnson and D. T. Sawyer, *Anal. Chem.*, 1984, **56**, 1890–1898.
37 C. Reichardt, *Chem. Rev.*, 2002, **94**, 2319–2358.
38 A. Kütt, S. Selberg, I. Kaljurand, S. Tshepelevitsh, A. Heering, A. Darnell, K. Kaupmees, M. Piirsalu and I. Leito, *Tetrahedron Lett.*, 2018, **59**, 3738–3748.
39 G. Jakab, C. Tancon, Z. Zhang, K. M. Lippert and P. R. Schreiner, *Org. Lett.*, 2012, **14**, 1724–1727.
40 J. F. Coetzee, *Prog. Phys. Org. Chem.*, 2007, **4**, 45–92.
41 I. M. Kolthoff and M. K. Chantooni, *J. Phys. Chem.*, 1968, **72**, 2270–2272.
42 R. Schwesinger and H. Schlemper, *Angew. Chem., Int. Ed. Engl.*, 1987, **26**, 1167–1169.
43 C. F. Bernasconi, A. E. Leyes, M. L. Ragains, Y. Shi, H. Wang and W. D. Wulff, *J. Am. Chem. Soc.*, 1998, **120**, 8632–8639.
44 P. Pramanik, R. Sahoo, S. Kumar Das and M. Halder, *Phys. Chem. Chem. Phys.*, 2020, **22**, 28045–28054.
45 Z. Rahman and S. K. Das, *ChemistrySelect*, 2021, **6**, 9164–9174.
46 J. T. Muckerman, J. H. Skone, M. Ning and Y. Wasada-Tsutsui, *Biochim. Biophys. Acta, Bioenerg.*, 2013, **1827**, 882–891.
47 M. J. Stirling, G. Sweeney, K. Macrory, A. J. Blacker and M. I. Page, *Org. Biomol. Chem.*, 2016, **14**, 3614–3622.
48 Z. Rahman, M. Rajbanshi, M. Mahato, S. Ghanta and S. Kumar Das, *J. Mol. Liq.*, 2022, **359**, 119365.